COBEM 2021 26th International Congress of Mechanical Engineering
November 22-26, 2021, Virtual Congress, Brazil

COB-2021- -2228
FULL THREE-DIMENSIONAL VERSUS THREE-DIMENSIONAL SYMMETRIC LAMINAR SWIRLING FLOW

Moisés Miranda
André Damiani
Universidade Federal do ABC – UFABC - Av. dos Estados, 5001 - Bangú, Santo André - SP, 09210-580
moises.miranda@ufabc.edu.br
a.damiani@ufabc.edu.br

Abstract. *Swirling flows are present in nature and in many engineering applications such as turbomachinery, combustion chambers, heat exchangers, and cyclone-type phase separators. The oil and gas industry demand for weight reduction and space occupied on offshore platforms has led to the development of compact separators, an axial inlet hydrocyclone, also known as an in-line separator. In this paper, the capability of the three-dimensional numerical model with periodic boundaries to predict physically realistic results is evaluated and compared with the fully three-dimensional model. The separator consists of a swirling device placed internally in a pipe. The pipe has 50 mm i.d. size and 2500 mm long pipe, and the swirling device is static, where twelve stationary vanes deflect the flow at an angle of 63.5º. Pressure drop, velocity field, vorticity distribution, swirl intensity, and decay were computed for numerical models, and the results were compared. The study considered the flow as laminar, single-phase, isothermal and steady-state. Single-phase flow was chosen to highlight the applications where there is one dispersed phase in the continuous phase, i.e., oil droplets in disposal water, after oil separation. Full hexahedral meshes were generated for the two models using ICEM-CFD, and the simulations were performed using Ansys® Fluent. The mesh of the three-dimensional model with periodic boundaries has approximately 1.13 million control volumes, while the fully three-dimensional model has about 13.5 million control volumes. Both models have been validated with results from the literature. Although the three-dimensional model with periodicity reduces the simulation time by approximately 93%, the model can predict physically realistic results only for $Re \leq 100$. The simplified model overestimated the swirl number by 34% for $Re = 250$ while underestimating the axial velocity by approximately 12% for $Re = 300$. It was observed a possible transition to an unsteady-state flow between the Reynolds numbers 250 and 300. This value is slightly lower than what is found in the literature and depends directly on the geometry of the swirl generator.*

Keywords: *Swirling Flow, In-line Separator, Computational fluid dynamics (CFD)*

1. INTRODUCTION

The separator vessels, which work through the gravitational principle, are still being applied in the oil industry. Nevertheless, their main project has not been changed lately. An increase in the separation vessel accompanies an increase in separation efficiency. Consequently, the increase in volume leads to an increase in weight which, in turn, requires an expansion of the platform to support the weight.

Hydrocyclones are an alternative lighter, more compact and the separation process is increased. The driving force is the centrifugal force generated by the tangential inlet, which creates the swirl velocity (Figure 1). The swirl velocity drives the heavier phase to the equipment wall, while the lighter phase is kept in the central part and collected by the reversal flow (Hayes et al., 1985).

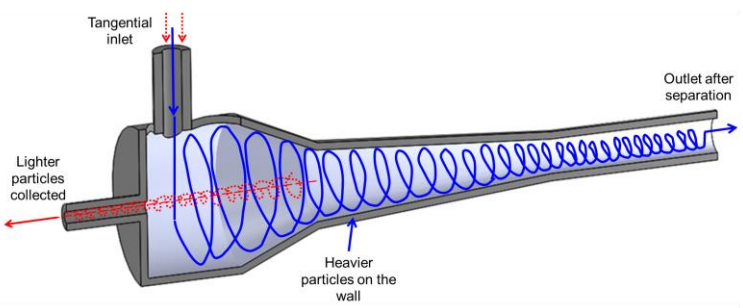

Figure 1. Schematic tangential hydrocyclone.

Alternatively, a more compact hydrocyclone is obtained when the flow enters axially, where static vanes promote the swirl. Regarding oil industry application, the flow behavior in an axial inlet hydrocyclone, also known as an in-line separator, was studied by several authors (Slot et al., 2011; van Campen et al., 2012; Steenbergen et al., 2015). Rocha (2015) study, the swirling flow was generated by a swirl generator device with 12 vanes, hemisphere nose upstream and conical trailing edge tail downstream (Figure 2). After the swirl generator device, a slice of the domain was simulated by CFD (Computational Fluid Dynamics) and compared to the experimental results.

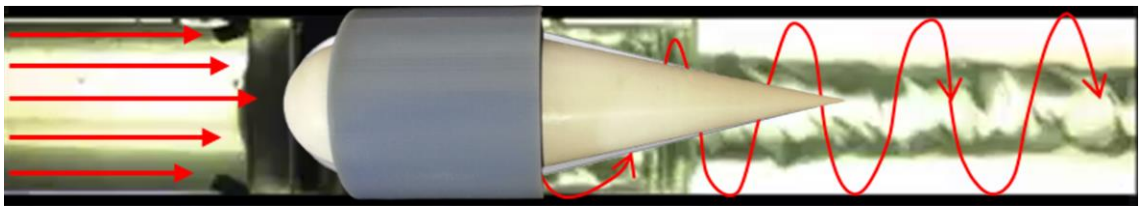

Figure 2. Axial inlet hydrocyclone (Rocha et al., 2015).

Swirling flow simulations are a challenge due to anisotropic patterns and pressure drops. Velocity gradients and strong tangential velocity lead to modification on streamlines and different vortex core patterns. This coupling between swirl and pressure field turns the numerical modeling complex. In a turbulent regime, the flow can be considered asymmetric for high slew intensities where the vortex breakdown occurs. Kitoh (1984) noted that even though the swirl is generated symmetrically, it develops asymmetrically to an interval of swirl intensity. For the laminar flow regime, most studies consider the two-dimensional and symmetrical flow (Crane and Burley, 1976; Singh et al., 1980; Rocha et al., 2015 and 2017).

In this context, this paper aims to compare the capability of the three-dimensional numerical model with periodic boundaries to predict physically realistic results and compare it with the fully three-dimensional model. Pressure drop, velocity field, vorticity distribution, swirl intensity, and decay were computed for numerical models in laminar single-phase swirling flow.

2. BACKGROUND

Vortex preset in the swirling flow was classified by Kundu and Cohen (2008) as solid-body / forced vortex, where the fluid elements behave as a solid body and rotate. The irrotational vortex or free vortex is irrotational everywhere, except in its origin, where the vorticity is infinity. The vorticity can be calculated from the curl of the velocity field.

$$\vec{\omega} = \nabla \times \vec{U} \tag{1}$$

Where the vorticity components in the cylindrical coordinate system are:

$$\vec{\omega}_r = \frac{1}{r}\frac{\partial w}{\partial \theta} - \frac{\partial v}{\partial z}, \qquad \vec{\omega}_\theta = \frac{\partial uv}{\partial z} - \frac{\partial w}{\partial r}, \qquad \vec{\omega}_z = \frac{1}{r}\frac{\partial rvu}{\partial r} - \frac{1}{r}\frac{\partial uv}{\partial \theta} \tag{2}$$

A cylindrical-coordinate system for a circular pipe internal flow was used (Figure 3), where: z, r and θ are the axial, radial and circumferential coordinate, respectively. In the same sequence, the velocity components w, v and u are axial radial and tangential velocities. Even though the component u in the direction θ be also called by azimuthal, circumferential or swirl velocity, all means tangential velocity which is used in this paper.

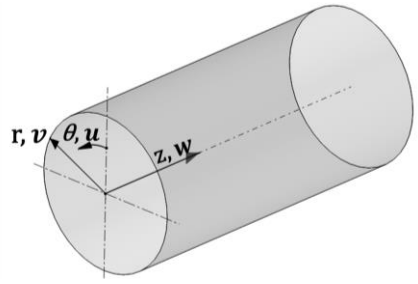

Figure 3. Cylindrical-coordinate system.

In swirl flows, it is common to associate the tangential component of velocity with a combination of a forced vortex and a free vortex. This profile is close to Rankine's idealized vortex. Figure 4a shows the forced vortex where the tangential velocity is proportional to the angular velocity (c'). Figure 4b shows the free vortex where the tangential velocity is inversely proportional to the radius. Figure 4c shows the combination of vortices.

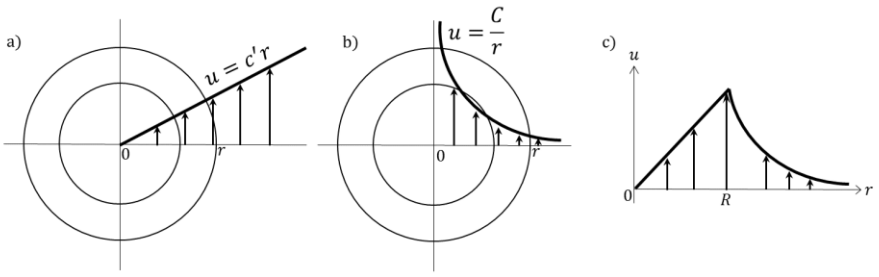

Figure 4. Rankine vortex.

From the tangential velocity distribution in swirling flow in circular duct Kitoh (1991) highlighted three distinct regions: wall, annular and central. On the wall, the velocity gradient is abrupt and less interesting. Annular and central regions are featured by free vortex and forced vortex, respectively. Gupta et al. (1984) affirmed that swirling flow always shows a central region of a forced vortex and a free vortex out of the central region.

Steenbergen and Voskamp (1998) classified typical conditions of turbulent swirling flow, depending on the swirl generator, in three different types: concentrated vortex (CV), solid body (SB) and wall jet (WJ), where rotations are concentrated near the center of the duct, uniform rotation and concentrated rotation near the wall, respectively. Typical swirl conditions in different equipment are shown with tangential velocity (u) on the vertical axis and internal radius (r) until maximum radius (R) on the horizontal direction (Figure 5).

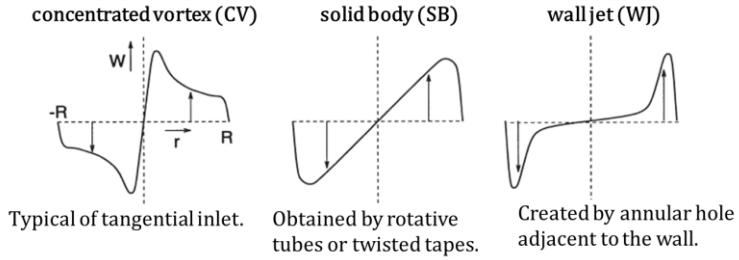

Figure 5. Classification of swirl types by Steenbergen and Voskamp (1998).

The swirling flow inside pipes presents swirl decay which is quantified by a nondimensional parameter called swirl number (S). Gupta et al. (1984) defined the swirl number as the axial flux of tangential momentum to the axial flux of axial momentum, times the equivalent nozzle radius.

$$S = \frac{\int_0^R ruwdA}{R\int_0^R wwdA} \tag{3}$$

By calculating S in different axial positions, it is possible to analyze the swirl decay. Dirkzwager (1996) stated that the swirl decay depends mainly on the Reynolds number (Re), the swirl number (S), inlet conditions and the pipe wall rugosity. The Reynolds number is defined as:

$$Re = \frac{\rho \bar{w} d}{\mu} \tag{4}$$

Where ρ,$\bar{w}$, d e μ are the density of the fluid, the average of axial velocity, the internal diameter of the pipe and dynamic viscosity, respectively.

2.1 Axial inlet hydrocyclone

Axial inlet hydrocyclone applied to particulates in the stream of air/gas has been established in the industry for more than 70 years (Strauss, 1975). Recently, many authors have investigated the application of axial inlet hydrocyclone to the oil industry, aiming low low-pressure drop and higher separation efficiency combined with the equipment's reduced size. Karimpoorheidari (2019) based on previous geometry and studies focused on numerical simulations of the turbulent flow promoted by the swirl generator device. For the geometry considered, the best performance might be achieved when the swirl number is 1.6. Furthermore, the author created a morphology prediction by CFD single-phase and domain after the swirl generator device, where the laminar steady-state condition lacked further investigations. Beaubert *et al.* (2015) conducted CFD studies of swirling flow created by swirl generator in single-phase laminar steady-state flow condition, where Re varying from 50 to 1,600 were evaluated. The domain considered was only a segment of the whole pipe and periodic boundary condition was applied on the interfaces. In this Re range, the maximum tangential velocity was reached nearly half of the radius distance of the pipe.

3. NUMERICAL MODELING

The governing equations for steady, three-dimensional, isothermal swirling flow in cylindrical coordinates are:

Continuity equation

$$\frac{1}{r}\frac{\partial(rv)}{\partial r}+\frac{1}{r}\frac{\partial(u)}{\partial\theta}+\frac{\partial(w)}{\partial z}=0 \tag{5}$$

r-momentum equation

$$v\frac{\partial v}{\partial r}+\frac{u}{r}\frac{\partial v}{\partial\theta}+w\frac{\partial v}{\partial z}-\frac{u^2}{r}=-\frac{\partial p}{\partial r}+\mu\left[\frac{\partial}{\partial r}\left(\frac{1}{r}\frac{\partial}{\partial r}(rv)\right)+\frac{1}{r^2}\frac{\partial^2 v}{\partial\theta^2}+\frac{\partial^2 v}{\partial z^2}-\frac{2}{r^2}\frac{\partial u}{\partial\theta}\right] \tag{6}$$

θ-momentum equation

$$v\frac{\partial u}{\partial r}+\frac{\partial u}{r}\frac{\partial u}{\partial\theta}+w\frac{\partial u}{\partial z}+\frac{vu}{r}=-\frac{1}{r}\frac{\partial p}{\partial\theta}+\mu\left[\frac{\partial}{\partial r}\left(\frac{1}{r}\frac{\partial}{\partial r}(ru)\right)+\frac{1}{r^2}\frac{\partial^2\theta}{\partial\theta^2}+\frac{2}{r^2}\frac{\partial u}{\partial\theta}\right] \tag{7}$$

z-momentum equation

$$v\frac{\partial w}{\partial r}+\frac{u}{r}\frac{\partial w}{\partial\theta}+w\frac{\partial w}{\partial z}=-\frac{\partial p}{\partial z}+\mu\left[\frac{1}{r}\frac{\partial}{\partial r}\left(r\frac{\partial w}{\partial r}\right)+\frac{1}{r^2}\frac{\partial^2 w}{\partial\theta^2}+\frac{\partial^2 w}{\partial z^2}\right] \tag{8}$$

Ansys Fluent® was the CFD software used and for the discretization of momentum equations, the method upwind second order was used, while for pressure interpolation PRESTO! (*PREssure STaggering Option*) was applied, which is highly recommended for swirling flow simulations. The SIMPLE (Semi Implicit Method for Pressure Linked Equations) method was used for velocity-pressure coupling.

3.1 Geometry

The geometry adopted in the present work was the axial inlet hydrocyclone and swirl generator device proposed by Rocha et al. (2015). The 3D computational domain was created, where the internal radius of the pipe (R_2) = 25 mm, entrance length (L_e) = 500 mm and the length L_s is 2,000 mm (Figure 6).

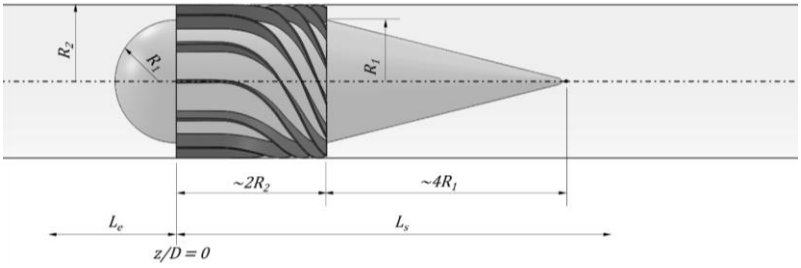

Figure 6. Geometry / computational domain.

Twelve static vanes are assembled on the solid body of radius R_1 = 20 mm, the deflection angle α is 63.5° (Figure 7).

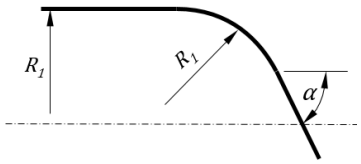

Figure 7. Schematic representation of the static vane.

3.2 Boundary conditions

The surfaces where the boundary conditions were applied are presented in Figure 8a. In the considered geometry, it is possible to observe physical repetitions of the segments of 30°. With the vane centered, periodic conditions could be applied on the interphases (Figure 8b). All the boundary conditions used are shown in Table 1.

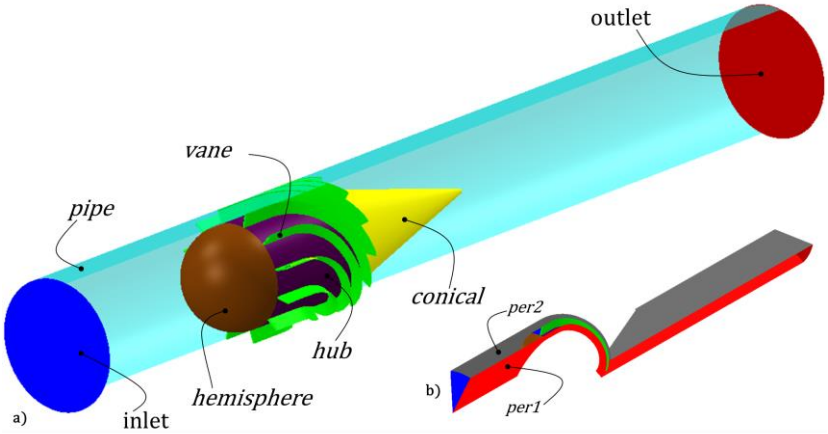

Figure 8. Boundary conditions.

Table 1. Boundary conditions.

surfaces	type	boundary condition
inlet	velocity	Depending on Re
outlet	pressure	0 [Pa]
pipe	wall	No slip
hemisphere	wall	No slip
vane	wall	No-slip
hub	wall	No-slip
conical	wall	No-slip
per1(1)	periodicity	
per2(1)	periodicity	

(1) only for simplified model

Uniform velocity was prescribed in the inlet and pressure in the outlet. The velocity inlet depends on the Re, where for 50 (U = 0.001 m/s), 100 (U = 0.002 m/s) e 250 (U = 0.005 m/s).

The working fluid was liquid water, where the properties are presented in Table 2.

Table 2. Fluid properties at 25°C.

Property	Value	Unit
Density	998.2	[kg/m³]
Dynamic viscosity	0.001003	[Pa.s]

3.3 Computational mesh

Taking the slice from the whole computational domain, the hexahedral meshes were generated using the software ICEM CFD for the periodic model (simplified model). The full mesh domain could be obtained by replicating 11 copies of the simplified model. Three meshes were generated with different degrees of refinement following the methodology recommended by Celik et al. (2008). Mesh quality regarding aspect ratio, orthogonal quality, skewness and ICEM quality showed suitable values. The definition of which mesh should be used was done through the grid independence test given by GCI (Grid Convergence Index). The GCI method proposed by Celik et al. (2008) consists of verifying how the significant parameters of the flow differ depending on the mesh refinement.

The average of different flow parameters following the equation (9) for Re = 250 and full model were evaluated in different section planes (Plane 1 = z/D = -0.5, Plane 2 = z/D = 0, Plane 3 = z/D = 1, Plane 4 = z/D = 3), where z = axial distance and D = pipe diameter, the origin of the domain (z/D = 0) is located in the vane entrance. Table 3 presents the GCI values for axial velocity. The Mesh 2 (Figure 9) which is the intermediate level of refinement with 13.5 million elements for the full domain and 1.13 million elements for the simplified model (1/12 of the full domain).

$$\frac{1}{A}\int \emptyset dA = \frac{1}{A}\sum_{i=1}^{n} \emptyset_i |A_i| \tag{9}$$

Table 3. GCI – Axial velocity.

Mesh	N. of elements	Plane 1 [cm/min]	Plane 2 [cm/min]	Plane 3 [cm/min]	Plane 4 [cm/min]
Mesh 1 - coarse	6,011,472	83.2	81.44	30.15	30.32
Mesh 2 - intermediate	13,545,240	81.77	81.25	30.17	30.14
Mesh 3 - fine	29,752,320	81.49	81.36	30.05	30.13
Extrapolated value[21]	-	83.58	81.71	30.14	30.33
GCI[21] [%]	-	0.57	0.4	0.016	0.041

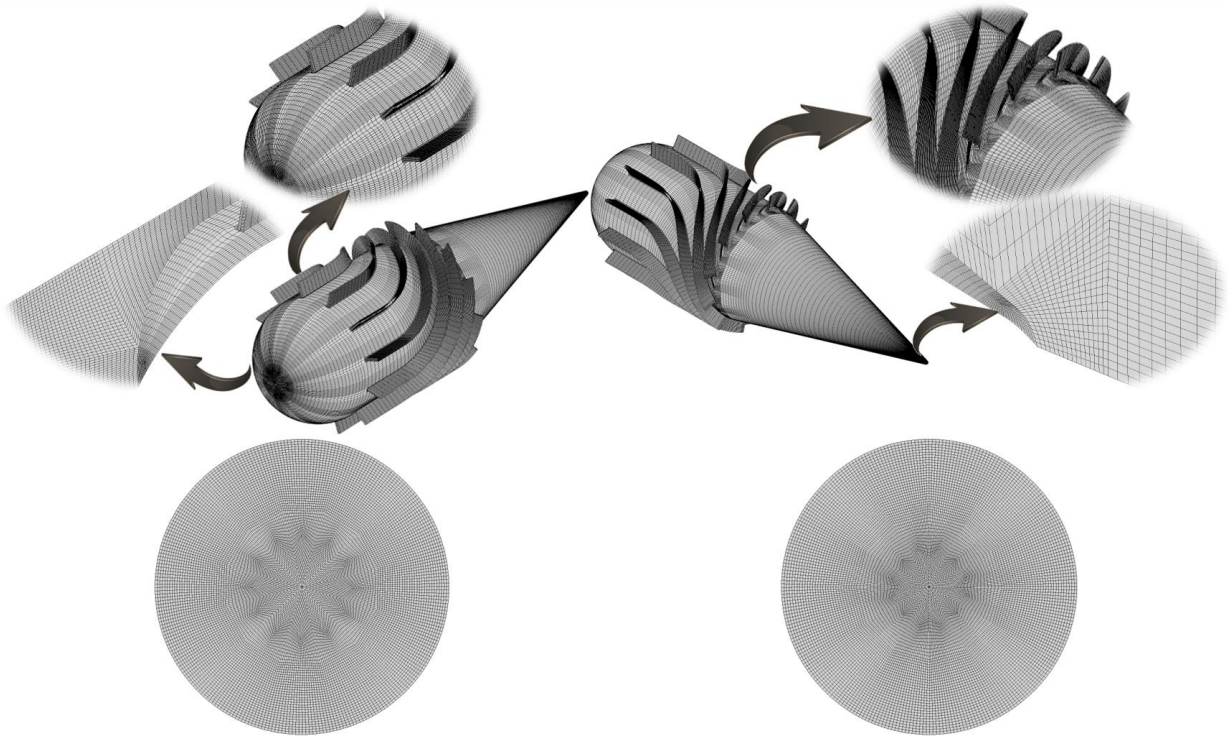

Figure 9. Hexa type Mesh 2 intermediate.

4. RESULTS AND DISCUSSION

The simulations were considered as converged when the residual values were lower than $1x10^{-6}$. Additionally, some parameters were monitored, such as the outlet's mass flow rate, which was considered converged when the variation was lower than 1%. For Re = 100, the simplified method took 2.5 hours to converge, while the full domain took 36 hours to converge. Thus, the simplified method reduced the simulation time by 93%. The fully developed axial velocity profile was compared between the models (the simplified and the full domain) and to the analytical result from the equation (10), which showed coincident results in Figure 10.

$$w = w_{max}\left(1 - \frac{r^2}{R^2}\right) \tag{10}$$

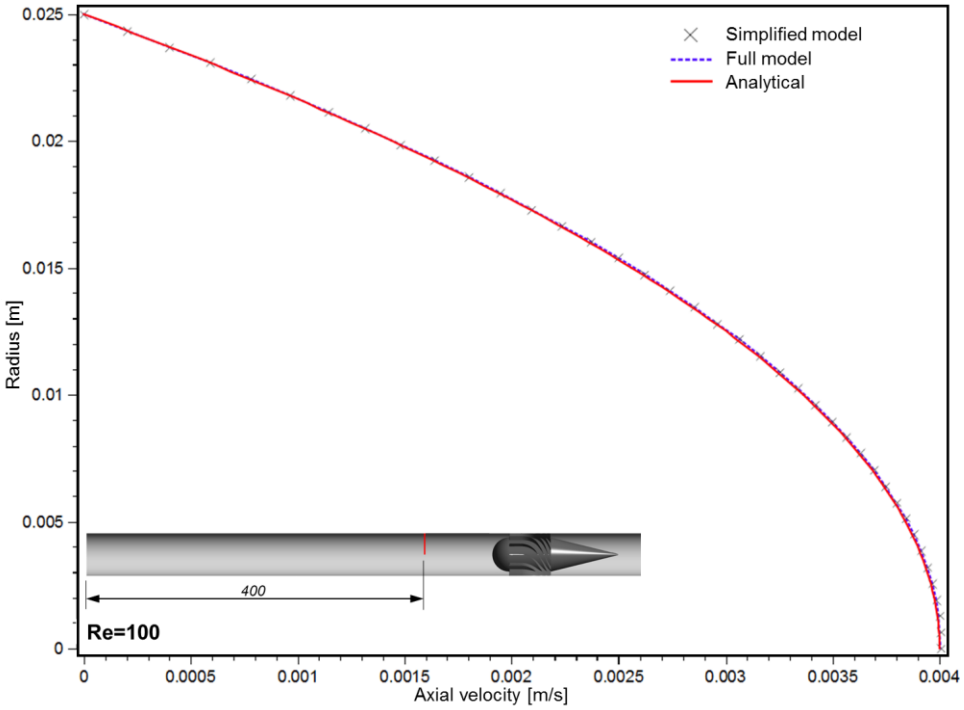

Figure 10. Fully developed axial velocity profile.

Longitudinal planes were generated in order to evaluate and compare the simplified model and the full model for Re = 50, 100 and 500. Although the simplified model uses only a segment of the whole domain, it can be represented as the whole domain by replicating the results. The results from the full domain are presented on the left side, while on the right side, the simplified model results are presented.

For Re = 50 (Figure 11a and Figure 11b) and Re = 100 (Figure 11c and Figure 11d) it is noticed that very similar are obtained on both models. In these cases, it is impossible to identify reverse flow (vectors) in the axial velocity results. While with the condition Re = 250 (Figure 10e and Figure 10f), reverse flow is presented and mainly on the results of axial and tangential velocity and vorticity the contours differ between the models, where the simplified model shows "smoother" plots. The length of the region in the pipe center with lower velocity is shorter with the full model for Re = 250.

Taking the section planes is possible to evaluate how the profiles are distributed on the cross-section of the pipe, starting from the axial velocity (

Figure 12). The low axial velocity on the core region is observed only for Re ≥ 100. For all simplified models, the axial velocity is distributed uniformly through the section and also for the full domain of Re = 50 and 100. It stands out the full domain of Re = 250 (

Figure 12e), where the axial velocity is not uniform in the annular region. This means that the simplified model with periodic boundary conditions is not able to capture the axial velocity structure in the annular region for Re ≥ 250.

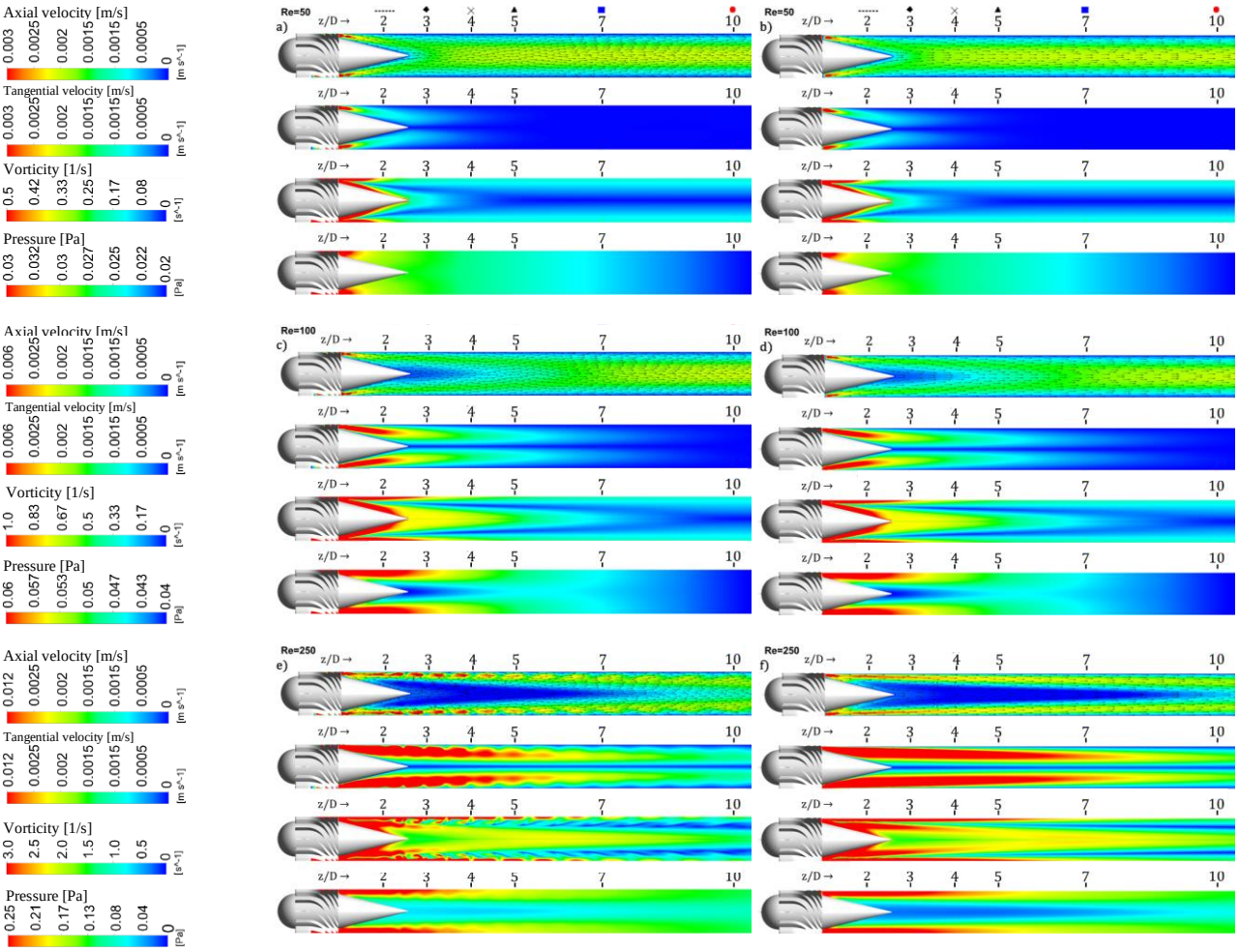

Figure 11. Longitudinal contours.

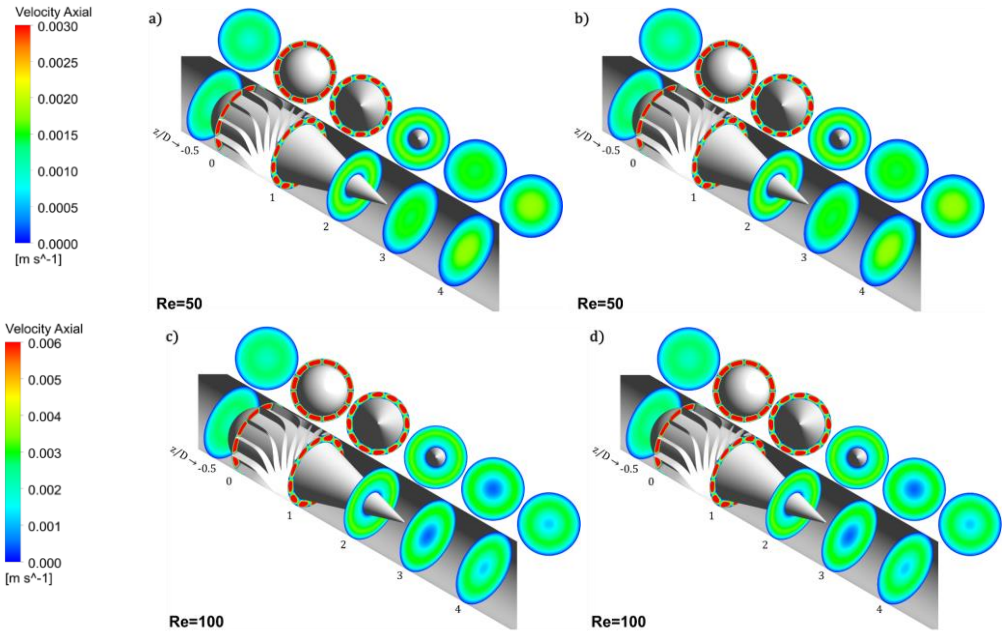

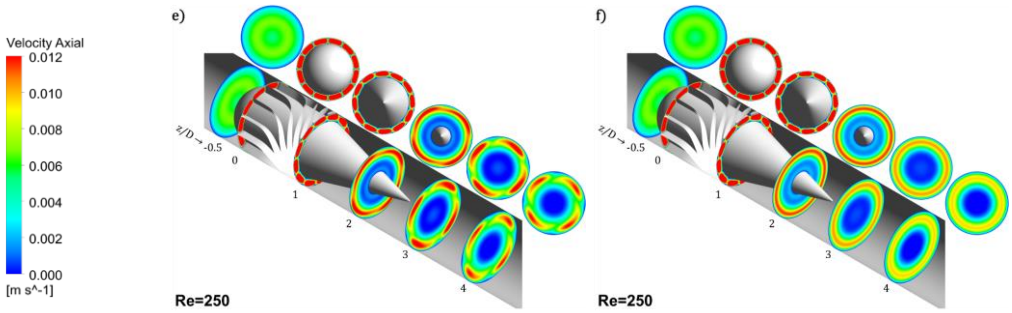

Figure 12. Cross-section axial-velocity contours.

The axial and tangential velocities and pressure profiles are presented in Figure 13. It was noticed that the profiles are equivalent when Re = 50 and 100, Re = 250 showed a more significant difference between the models. Axial velocity in the central region of the full domain predicted higher values, clearly seen in the distance z/D = 5, where the axial velocity is twice of the simplified model at the R = 0.

The simplified model predicted higher maximum tangential velocity in the annular region, mainly in z/D = 5. The pressure drop in the section is higher with the simplified domain, where shows lower pressure in the center and higher pressure next to the pipe wall. It happens because the radial pressure in the free vortex is directly proportional to the square of tangential velocity and inversely proportional to the pipe radius.

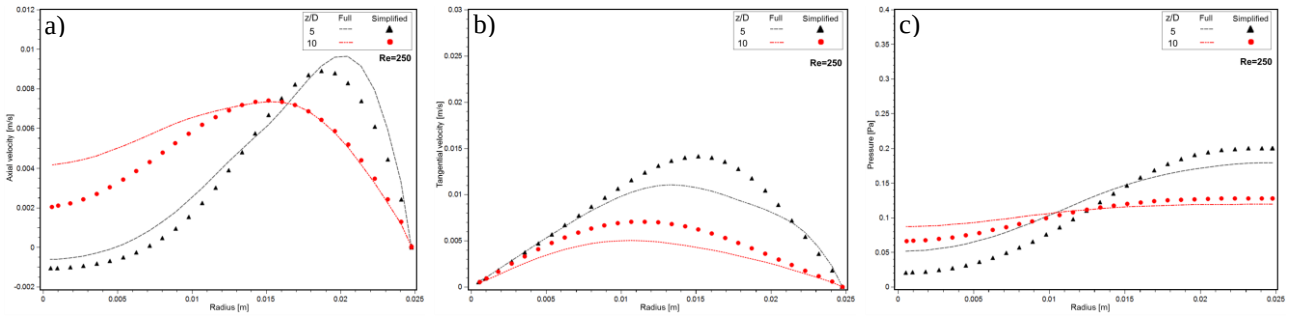

Figure 13. Re = 250 results profiles.

When the Swirl number S is calculated, the swirl decay profile could be obtained for Re = 50, 100 and 250 (Figure 14). Regarding Re = 50, Swirl Number is approximately zero in the position z/D = 5 and for Re = 100 z/D = 10. This means that the tangential velocity is fully dissipated due to the viscous effect after 5 and 10 times the diameter of the pipe when the Re is low. While for Re = 250, the distance of z/D = 20 is not enough to fully dissipate the tangential velocity. In this flow condition, the swirl number is overestimated by 34% in the simplified domain; however, when it approaches the outlet, the values are getting close.

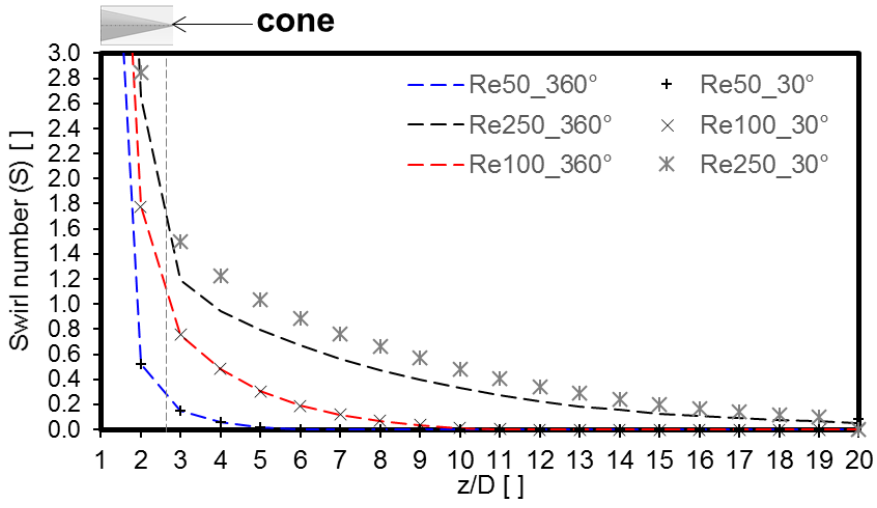

Figure 14. Swirl number.

Aiming to find where the transition between the steady-state and unsteady-state, the Re = 300 was considered and having the swirl number after the cone trailing edge over the number of iteration, the variation of the swirl number is still seen even after a high number of iterations (Figure 15b), while for Re = 250 the number of swirl got stable in a reduced number of iterations (Figure 15a).

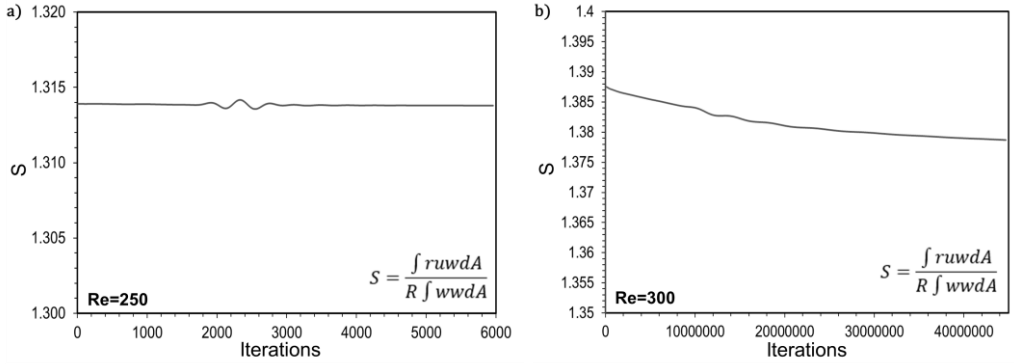

Figure 15. Swirl number over iterations for Re = 250 and Re = 300.

5. CONCLUSIONS

The axial inlet hydrocyclone with full hexahedral mesh was evaluated via CFD for single-phase, laminar, steady-state condition and the full domain was compared to the simplified model considering the periodic boundary condition, widely applied to turbomachinery simulations. The outputs showed that for low Reynolds numbers (Re = 50 and 100), the results are very accurate. However, for Re ≥ 250, the velocities profiles are not coincident but still can be used as estimation by significantly reducing the computational effort. Even in the laminar regime, the unsteady-state might be predominant for Re > 250.

6. REFERENCES

Beaubert, F., Pálsson, H., Lalot, S., Choquet, I., Bauduin, H., 2015. “Design of a device to induce swirling flow in pipes: A rational approach”, Comptes Rendus - Mecanique, 343(1), pp. 1–12.

van Campen, L. J. A. M., Mudde, R. F., Slot, J. J., Hoeijmakers, H. W. M., 2012. “A Numerical and Experimental Survey of a Liquid-Liquid Axial Cyclone”. International Journal of Chemical Reactor Engineering, 10(1).

Celik, I. B, Ghia, U., Roache, P. J., Freitas, C. J., Coleman, H., Raad, P. E., 2008. “Procedure for Estimation and Reporting of Uncertainty Due to Discretization in CFD Applications”. Journal of Fluids Engineering, 130(7), pp. 1-4.

Crane, C. M. and Burley, D. M., 1976. “Numerical studies of laminar flow in ducts and pipes”, Journal of Computational and Applied Mathematics, 2(2), pp. 95–111.

Dirkzwager, M., 1996. “A New Axial Cyclone Design for Fluid-Fluid Separation’. Ph.D. Thesis. Delft University of Technology, Delft, Netherlands.

Gupta, A. K. Lilley, D. G., Syred, N., 1984. “Swirl flows”. Abacus Press, Tunbridge Wells, England.

Hayes, J. J., Carroll, W. C., Fothergill, D. W. J., Prendergast, G. J. J. “Hydrocyclones for treating oily water: Development and field testing in bass strait”. Proceedings of the Annual Offshore Technology Conference. Offshore Technology Conference, pp. 549–556.

Karimpoorheidari, A., 2019. “A Numerical Study of Swirl Flow in Pipes”. MSc. Thesis. Delft University of Technology, Delft, Netherlands.

Kitoh, O., 1984. “Axi-asymmetric Character of Turbulent Swirling Flow in a Straight Circular Pipe”. Bulletin of JSME, 27(226), pp. 683–690.

Kitoh, O., 1991. “Experimental study of turbulent swirling flow in a straight pipe”. Journal of Fluid Mechanics, 225, pp. 445-479.

Kundu, P. K. and Cohen, I. M., 2008. Fluid Mechanics. 4th edn, Journal of Chemical Information and Modeling. 4th edn. Elsevier.

Rocha, A. D., Bannwart, A. C. and Ganzarolli, M. M., 2015. “Numerical and experimental study of an axially induced swirling pipe flow”. International Journal of Heat and Fluid Flow. Elsevier, pp. 81–90.

Rocha, A. D., Bannwart, A. C. and Ganzarolli, M. M., 2017. “Effects of inlet boundary conditions in an axial hydrocyclone”. Journal of the Brazilian Society of Mechanical Sciences and Engineering 2017 39:9, 39(9), pp. 3425–3437.

Singh, M. P., Sinha, P. C. and Aggarwal, M., 1980. “Swirling Flow in a Straight Circular Pipe”. ZAMM - Journal of Applied Mathematics and Mechanics / Zeitschrift für Angewandte Mathematik und Mechanik, 60(9), pp. 429–436.

Slot, J. J., van Campen, L. J. A. M., Hoeijmakers, H. W. M., Mudde, R. F., 2011. “In-line oil-water separation in swirling flow”. In the 8th International Conference on CFD in Oil & Gas, Metallurgical and Process Industries SINTEF/NTNU, Trondheim NORWAY, (June), pp. 1–10.

Steenbergen, W. and Voskamp, J., 1998. “The rate of decay of swirl in turbulent pipe flow”. Flow Measurement and Instrumentation, 9(2), pp. 67–78.

Strauss, W., 1975. Industrial Gas Cleaning: The Principles and Practice of the control of gaseous and particles emissions. Second edi. Pergamon Press, United States.

7. RESPONSIBILITY NOTICE

The authors are the only responsible for the printed material included in this paper.